Characterization of Atrial Spatiotemporal Dynamics for Prediction of Atrial Fibrillation Recurrence after Ablation

Hugo Hernández-Alemán[1], Carlos Sánchez[1,3], Ana Mincholé[1,3], Javier Ramos-Maqueda[2], Jorge Melero-Polo[2], Juan Pablo Martínez[1,3], Esther Pueyo[1,3]

[1] BSICoS Group, I3A, IIS Aragón, Universidad de Zaragoza, Zaragoza, Spain
[2] Clinical Hospital Lozano Blesa, Zaragoza, Spain
[3] CIBER en Bioingeniería, Biomateriales y Nanomedicina (CIBER-BBN), Zaragoza, Spain

Abstract

Atrial fibrillation (AF) is the most common sustained arrhythmia worldwide, increasing the risk of stroke, heart failure, and mortality. Pulmonary vein ablation, which is usually combined with electroanatomical mapping (EAM) recording, is a key treatment for AF, but the high rate of recurrence after ablation remains a significant challenge. This study characterizes atrial regions associated with arrhythmic substrates using conventional electrogram (EGM) markers, such as peak-to-peak voltage or fractionation, as well as new approaches based on EGM morphology using Principal Component Analysis.

The atrial geometries of 45 patients were segmented using a K-Means-based mesh division in pre-ablation EAMs. Regional EGM markers were then quantified and their statistics analyzed within each region. Our results show significant differences in these markers between patients with and without AF recurrence. Patients with AF recurrence exhibited lower voltages (0.98 vs 1.8), higher fractionation (9.29 vs 5.45), greater EGM morphological variability (0.53 vs 0.61), and increased complexity (55.71 vs 70.78 in r_σ^1 and 20.25 vs 12 in K), all of which can contribute to arrhythmogenesis. These findings highlight the potential of these markers to predict AF recurrence and guide personalized treatment.

1. Introduction

Atrial fibrillation (AF) is the most common sustained cardiac arrhythmia and a highly prevalent disease. AF is progressive, with paroxysmal episodes becoming more frequent and persistent, which over time can become permanent [1]. AF management represents a significant challenge, and current research focuses on better understanding its mechanisms, progression, and treatment options [**?**].

Catheter ablation is a widely used treatment strategy for AF. Pulmonary vein isolation (PVI) is the most commonly used approach, electrically disconnecting these veins from the left atrium and returning patients to sinus rhythm. Unfortunately, a significant proportion of treated patients (10%-35%) experience recurrence after ablation. In addition, no significant reduction in the recurrence rate of AF is observed when second ablations are performed [2].

Although PVI remains the cornerstone of AF ablation, attention has also been paid to the identification of additional arrhythmogenic targets beyond the pulmonary veins, such as the left atrial appendage [3] and the posterior wall [4], as potential sources for the initiation and maintenance of AF. Electroanatomical mapping (EAM) has been developed to better understand and ablate complex AF substrates, identifying low voltage areas, fibrosis, reentry circuits, and rotational drivers [5].

Current studies focus on extracting important information from the EAM. Processing of associated electrograms (EGMs) has led to the calculation of maps that represent peak-to-peak voltage [6, 7], fractionation [8], and conduction velocity [9]. In addition, specific EGM morphologies have been analyzed to identify electrophysiological mechanisms such as pivot sites, wavefront collisions, and conduction gaps [8, 10]. Patients with AF recurrence often exhibit lower voltage, slower conduction, and greater fractionation, reflecting underlying atrial remodeling. While these markers provide valuable information, they may not fully capture the complexity and heterogeneity of atrial EGM features that are critically associated with AF recurrence.

In this study, our objective is to go beyond conventional metrics by performing a detailed local analysis of EGM morphology and signal complexity. Specifically, we propose and evaluate markers that quantify spatial heterogeneity and fragmentation to improve substrate characterization. This allows for the distinction between patients with and without AF recurrence following PVI, providing a clearer understanding of the electrophysiological remodeling underlying arrhythmogenic substrates.

2. Materials and methods

2.1. Database

In this study, we analyzed the EAM and EGM recordings of 45 patients with AF who underwent their first PVI procedure at Hospital Clínico Universitario Lozano Blesa, Zaragoza (Spain). Six of them (13.33%) experienced recurrence within 12 months after ablation. Three-dimensional atrial geometry and high density mapping (HDM) data were acquired before and after ablation with an HDM system (Rhythmia; Boston Scientific Corporation, Marlborough, MA) and a basket-type catheter (INTELLAMAP ORION™ Mapping Catheter; Boston Scientific). In this work, we analyzed preablation maps, as they provide higher mesh quality than postablation maps and cover not only the pulmonary veins but also the entire atria. EAMs include an average of 8309 ± 3051 recorded EGMs along with the corresponding ablation lines.

2.2. EGMs and mesh processing

HDM data were processed using MATLAB. The unipolar EGMs, initially recorded at a sampling frequency of 953.674 Hz, were bandpass filtered between 30 and 300 Hz. In the atrial meshes, pulmonary veins were excluded following the ablation lines, resulting in maps with an average of 3,586 ± 1,519 EGMs. All EGMs were aligned using cross-correlation, a necessary step to calculate the markers described in the following section. To perform a local analysis of the electrical activity of the atria, we divided each mesh into *k* regions of approximately the same size, treating each region as a cluster of mesh nodes c_j. *K-Means* algorithm was used to initially assign *k* random centroids on the mesh. Then, vertices x_i were assigned to the nearest centroid based on the Euclidean distance, and the centroids were recalculated as the mean of the points S_j within each cluster:

$$x_i \to S_{j^*}, \quad s.t. \quad j^* = \arg\min_j \|x_i - c_j\|^2 \tag{1}$$

$$c_j = \frac{1}{|S_j|} \sum_{x_i \in S_j} x_i. \tag{2}$$

This process was repeated until the centroids no longer changed significantly. We conducted several analyses that divided the maps into 40 to 100 regions or clusters. The regions in each map with fewer than 5 EGMs were discarded to avoid highly unequal distributions of the recordings across the mesh.

2.3. EGM markers

The following markers were calculated from the unipolar EGM signals of each patient:

- Peak-to-peak voltage V_{p-p}, defined as the difference between the maximum and minimum values of the activation waveform of each EGM.
- Fractionation index *F*, defined as the number of peaks in amplitude-normalized EGMs whose absolute value exceeds 0.3, a threshold chosen to effectively separate true peaks from background noise.
- EGM similarity ρ, defined as the average of the Pearson correlation coefficients computed between each EGM and the rest of the EGMs in the same region.

Furthermore, for each patient, we identified the EGMs associated with healthy tissue by selecting the EGMs with bipolar V_{p-p} greater than 0.5 mV, as in previous studies [11]. A spatial transformation was applied to these EGMs using Principal Component Analysis (PCA). This resulted in the transformation matrix V. The coefficients of the original EGMs X expressed as linear combinations of the principal component basis were defined as $Z = V^T X$.

The proportion of variance in X that is explained by the first *k* components, $r_\sigma^{1\dots k}$, is measured for each EGM as the ratio between the sum of the squares of the transformed coefficients Z_j (scores in the *j*-th principal component) in the first *k* components to the total signal variance:

$$r_\sigma^{1\dots k} = \frac{\sum_{j=1}^{k} Z_j^2}{\sum_{j=1}^{N} Z_j^2} \cdot 100. \tag{3}$$

where N is the total number of principal components. This calculation quantifies how much of the variance can be explained by the first three components (r_σ^1, r_σ^{12}, r_σ^{123}).

The first three components leave a substantial portion of variance unexplained, which indicates a greater heterogeneity and requires more principal components for an accurate representation. For this reason, an additional marker, K, which represents the number of components k required to explain 90% of the variance in each region was calculated:

$$K = \min\{k \mid r_\sigma^{1\dots k} \geq 90\%\}. \tag{4}$$

For each of the seven markers, a unique representative value per region was computed as the average of the marker's values of the EGMs in that region. Therefore, for each region $m = 1 \dots M$, we obtain $V_{p-p}(m)$, $F(m)$, $\rho(m)$, $r_\sigma^1(m)$, $r_\sigma^{12}(m)$, $r_\sigma^{123}(m)$ and $K(m)$.

2.4. Statistics

For each patient and EGM marker, the median value in all regions was calculated to obtain a unique marker value per patient. The Mann-Whitney U test was used to test differences in the values of each marker between patients with and without AF recurrence. The values in each group are given as median [IQR]. Differences were considered statistically significant if the p-value was less than 0.05.

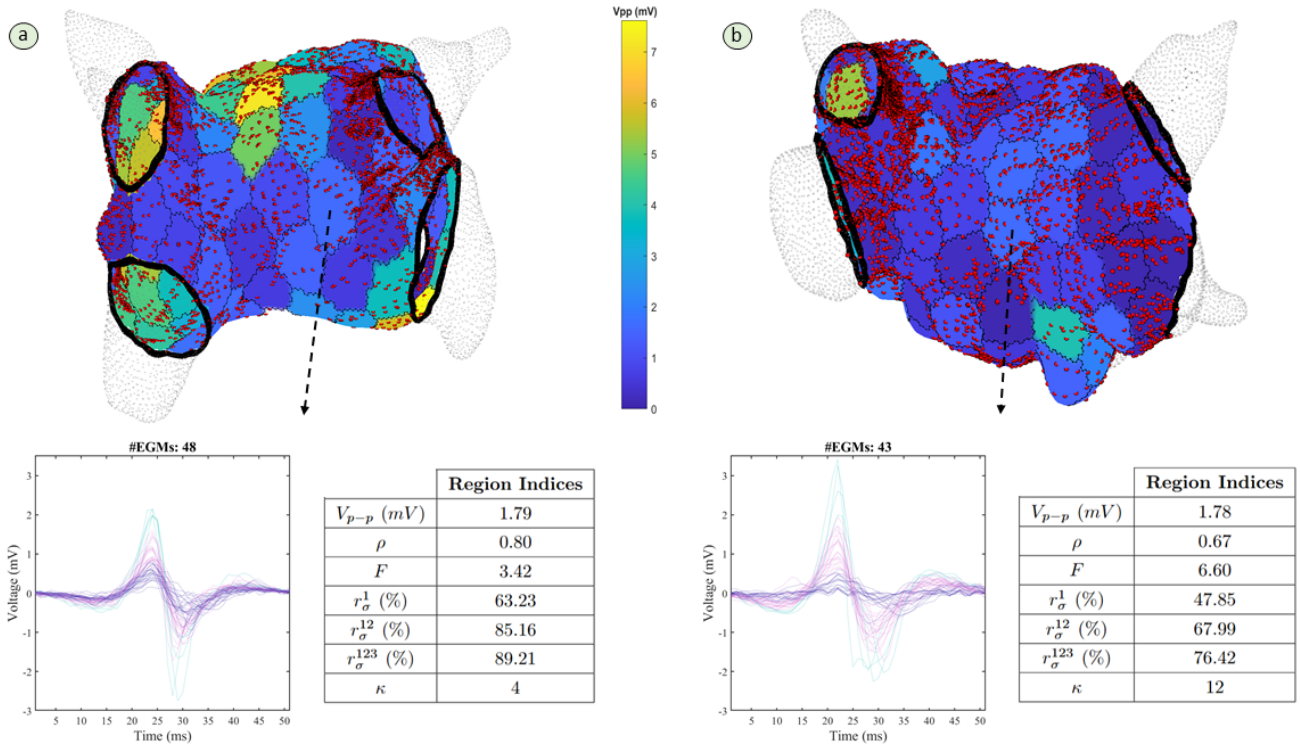

	Region Indices
V_{p-p} (mV)	1.79
ρ	0.80
F	3.42
r_σ^1 (%)	63.23
r_σ^{12} (%)	85.16
r_σ^{123} (%)	89.21
κ	4

	Region Indices
V_{p-p} (mV)	1.78
ρ	0.67
F	6.60
r_σ^1 (%)	47.85
r_σ^{12} (%)	67.99
r_σ^{123} (%)	76.42
κ	12

Figure 1. Example of V_{p-p} maps for a patient without AF recurrence (a) and one with AF recurrence (b). Red dots represent EGM recording locations. EGMs in a region are shown. The averaged values in the region of the seven computed markers are displayed in the tables below.

3. Results

The meshes were divided into N regions, with N ranging from 40 to 100, with an average surface area per region ranging from 2.03 to 1.01 cm², respectively. Consistent results were obtained for all tested numbers and, thus, the results are subsequently presented only for N=90 regions. Figure 1 shows V_{p-p} maps of a patient without (a) and a patient with (b) AF recurrence, along with examples of two regions of similar V_{p-p} values and their seven computed indices.

Figure 2 shows the differences between the two groups of patients for the seven markers derived from the EGM analysis. Patients without AF recurrence exhibited significantly higher V_{p-p} values (1.8 [1.21] vs 0.98 [0.62], $p = 0.007$). Furthermore, the similarity index ρ was significantly lower in the recurrence group (0.61 [0.11] vs 0.53 [0.07], $p = 0.016$). EGM fractionation ((F) was markedly higher in patients with recurrence (5.45 [2.78] vs 9.29 [2.23], $p = 0.014$). PCA-based variance markers (r_σ^1, r_σ^{12}, r_σ^{123}) showed a decrease in the AF recurrence group, with the largest differences found for r_σ^1 (70.78 [10.80] vs 55.71 [8.09], $p < 0.01$). In line with these results, K was significantly higher in patients with recurrence (12 [5.38] vs 20.25 [4], $p = 0.005$).

4. Discussion

In this study, we show that markers derived from pre-ablation EAM and UHD data can be used to separate the groups of patients with and without AF recurrence.

Lower V_{p-p}, higher fractionation and increased morphological variability of EGMs in patients with AF recurrence point to more severe tissue remodeling and arrhythmogenic substrates. In contrast, patients without recurrence exhibited significantly higher V_{p-p}, suggesting healthier tissue with lower accumulation of fibrosis. Furthermore, lower ρ values and higher F in the recurrence group reflect greater spatial variability and signal fragmentation, indicative of conduction abnormalities.

The PCA-based markers provide further insight into these differences. Patients with AF recurrence showed lower r_σ^1, r_σ^{12}, r_σ^{123} values, indicating that atrial EGMs in these patients require more principal components (calculated from tissues identified as healthy) to explain the same amount of variance. This suggests that atrial EGMs in recurrent patients are less spatially coherent and more heterogeneous than those in non-recurrent patients, reflecting a more complex and disorganized atrial substrate. This is supported by the higher values of K observed in the recurrence group, indicating increased signal complexity con-

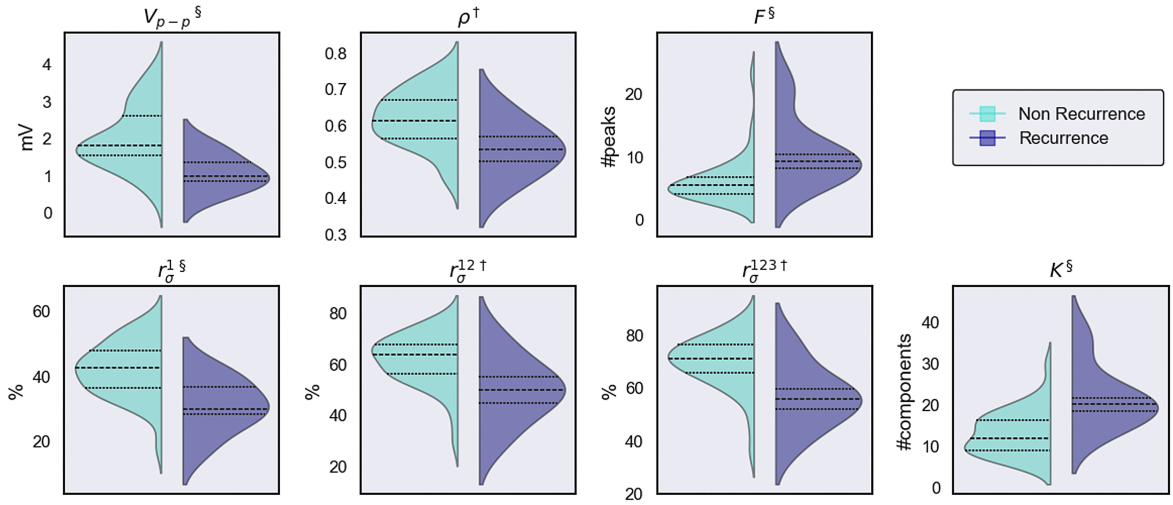

Figure 2. Statistical distributions of EGM-derived markers in the groups of patients with (dark blue) and without (turquoise) AF recurrence. Median, Q1 and Q3 values are indicated by dashed lines. §: $p < 0.01$; †: $p < 0.05$.

sistent with the regional fragmentation seen in these patients.

Acknowledgments

Funding was provided by projects PID2022-140556OB-I00, PID2023-148975OB-I00, CNS2022-135899, and TED2021-130459B-I00 (Agencia Estatal de Investigación, Ministerio de Ciencia y Innovación), BSICoS group T39_23R (Aragón Government). The calculations were performed using ICTS NANBIOSIS (HPC Unit at University of Zaragoza).

References

[1] Ball J, Carrington MJ, McMurray JJ, Stewart S. Atrial fibrillation: Profile and burden of an evolving epidemic in the 21st century. International Journal of Cardiology 2013; 167(5):1807–1824. ISSN 0167-5273.

[2] Mulder B, et al. Identifying patients with atrial fibrillation recurrences after two pulmonary vein isolation procedures. Open Heart Dec 2021;8(2):e001718.

[3] Romero J, Natale A, Di Biase L. Atrial fibrillation ablation beyond pulmonary veins: The role of left atrial appendage. Revista Portuguesa de Cardiologia Nov 2017; 36(Suppl 1):31–41.

[4] Kistler P, et al. Effect of catheter ablation using pulmonary vein isolation with vs without posterior left atrial wall isolation on atrial arrhythmia recurrence in patients with persistent atrial fibrillation: The capla randomized clinical trial. Journal of American Medical Association Jan 2023; 329(2):127–135.

[5] Fiedler L, et al. Characterization of high-density mapping in catheter ablation for persistent atrial fibrillation: results from the advisor™ hd grid mapping catheter observational study. Journal of Interventional Cardiac Electrophysiology 12 2022;66.

[6] Ballesteros G, et al. Association of left atrium voltage amplitude and distribution with the risk of atrial fibrillation recurrence and evolution after pulmonary vein isolation: An ultrahigh-density mapping study. Journal of Cardiovascular Electrophysiology Aug 2019;30(8):1231–1240.

[7] Lahuerta A, et al. Atrial low voltage areas: A comparison between atrial fibrillation and sinus rhythm. Cardiology Journal 2022;29(2):252–262.

[8] Frontera A, et al. Electrogram fractionation during sinus rhythm occurs in normal voltage atrial tissue in patients with atrial fibrillation. Pacing and Clinical Electrophysiology Feb 2022;45(2):219–228.

[9] Heida A, et al. Reduction of conduction velocity in patients with atrial fibrillation. Journal of Clinical Medicine Jun 2021;10(12):2614.

[10] Frontera A, et al. Electrogram signature of specific activation patterns: Analysis of atrial tachycardias at high-density endocardial mapping. Heart Rhythm 2018;15(1):28–37. ISSN 1547-5271.

[11] Schreiber D, et al. Catheter ablation of atrial fibrillation with box isolation of fibrotic areas: Lessons on fibrosis distribution and extent, clinical characteristics, and their impact on long-term outcome. Journal of Cardiovascular Electrophysiology 2017;28(9):971–983.

Address for correspondence:

Hugo Hernández-Alemán
Universidad de Zaragoza, Campus Río Ebro, I3A, D-6.01.1B, C. Mariano Esquillor, s/n, 50018 Zaragoza (Spain).
hhernandez@unizar.es